Talanta 196 (2019) 197–203

Contents lists available at ScienceDirect

Talanta

journal homepage: www.elsevier.com/locate/talanta

Photoelectrochemical biosensor for protein kinase A detection based on carbon microspheres, peptide functionalized Au-ZIF-8 and TiO_2/g-C_3N_4

Yue Wang[a], Xue Li[a], Geoffrey I.N. Waterhouse[a,b], Yunlei Zhou[a,*], Huanshun Yin[a,*], Shiyun Ai[a]

[a] College of Chemistry and Material Science, Shandong Agricultural University, 271018 Taian, Shandong, People's Republic of China
[b] School of Chemical Sciences, The University of Auckland, Auckland 1142, New Zealand

ARTICLE INFO

Keywords:
Photoelectrochemical biosensor
TiO_2-g-C_3N_4
Au-ZIF-8
Inhibition

ABSTRACT

In this work, a novel and sensitive photoelectrochemical (PEC) strategy was designed for protein kinase A (PKA) detection, comprising carbon microsphere (CMS) modified ITO electrode, TiO_2 as the phosphate group recognition material and graphite-carbon nitride (g-C_3N_4) as photoactive material. For the first time, gold nanoparticle decorated zeolitic imidazolate frameworks (Au-ZIF-8) was employed to fabricate biosensor for PKA activity assay with the function of substrate peptide immobilization and signal amplification. Firstly, substrate peptides were assembled on the Au-ZIF-8/CMS/ITO surface through the covalent bonding between the gold nanoparticles (AuNPs) and sulfydryl groups of the peptides. Then, in the presence of ATP, phosphorylation of the substrate peptide was achieved under PKA catalysis. Finally, TiO_2-g-C_3N_4 composites were further modified on the electrode surface based on bonding between TiO_2 and phosphate groups created via phosphorylation of the peptide (yielding TiO_2-g-C_3N_4/P-peptide/Au-ZIF-8/CMS/ITO), which is different with our previous work by directly immobilizing g-C_3N_4 composite on electrode surface. The developed method showed a wide linear range from 0.05–50 U mL^{-1}. The detection limit was 0.02 U mL^{-1} (S/N = 3). The constructed biosensor exhibited high detection specificity for PKA. In addition, the wide applicability of this biosensor was demonstrated by evaluating the inhibition ability of ellagic acid towards PKA.

1. Introduction

Protein kinase A (PKA) catalyzes phosphorylation modification of protein by transferring ATP terminal phosphate to serine or threonine residues. Activation of PKA mediates different responses of cells to external signals such as proliferation, ion transport, metabolic regulation and gene transcription [1]. The aberrant expression of protein phosphorylation is closely related to various serious illnesses, including cancer, inflammation, heart disease and senile dementia [2]. Accordingly, protein kinase is an important pharmaceutical target to cure severe diseases causing by abnormal levels of protein phosphorylation [3]. To realize the relationship between disease and protein kinase (including molecular mechanisms), and allow the development of protein kinase specific drugs, simple and sensitive method for protein kinase measurement must be discovered.

Existing methods for determining protein kinase activity include mass spectroscopy [4], fluorescence [5,6], colorimetry [7,8], Raman spectroscopy [9], surface plasmon resonance imaging [10], electrochemistry [11–13], electrochemiluminescence (ECL) [14] and photoelectrochemical (PEC) method [15,16]. Amongst these, PEC methods have drawn much interest due to the numerous advantages including excellent sensitivity, low background interference and low cost. The PEC process relies on light absorption by a semiconducting photoactive material which results in the charge separation (i.e. when $E > E_g$, electron can be excited from valence band into the conduction band of the semiconductor, which will lead to leave a hole in the valence band), followed by subsequent charge transfer to an electrode giving a measurable current [17]. For PEC analyses, choice of photoactive material is crucial for sensor fabrication. To date, many semiconductor nanomaterials have been successfully employed in PEC sensors, including TiO_2, ZnS, BiOI, ZnO, $ZnIn_2S_4$, CdS quantum dots (QDs), CdSe QDs, CdTe QDs, N-doped graphene QDs, and graphitic-like carbon nitride (g-C_3N_4) [18–20]. Whilst these photoactive materials have been successfully used in biosensor fabrication, some contain toxic elements which is undesirable. Accordingly, g-C_3N_4 is a particularly attractive material to use in PEC biosensor development due to its low cost, lightweight, ease of synthesis and good photocatalytic activity under visible light (E_g ~ 2.7 eV). Due to these properties, g-C_3N_4 is now finding widespread application in the field of catalysis, sorption, solar cell devices and analytical analyses, especially PEC analysis as photoactive material

* Corresponding authors.
E-mail addresses: zhyl@sdau.edu.cn (Y. Zhou), yinhs@sdau.edu.cn (H. Yin).

https://doi.org/10.1016/j.talanta.2018.12.035
Received 13 August 2018; Received in revised form 4 December 2018; Accepted 11 December 2018
Available online 12 December 2018
0039-9140/

[21–23]. However, bare g-C_3N_4 shows only modest photoactivity under visible light due to rapid electron-hole pair recombination following photoexcitation. To overcome this limitation, g-C_3N_4 is frequently combined with other materials to facilitate effective charge separation, for instance g-C_3N_4/graphene, g-C_3N_4/CuS and g-C_3N_4/TiO_2, wherein conduction band electrons in g-C_3N_4 typically migrate across heterojunctions onto the other material, thus preventing electron-hole pair recombination in g-C_3N_4 [24,25]. TiO_2 has been widely used in sensor development, offering the advantages of high activity under UV excitation, high chemical stability, nontoxicity, large surface area, commercial availability and easy synthesis. Nevertheless, the wide band gap (3.0–3.2 eV) limits its application in PEC biosensors because the UV light required for photoexcitation is harmful to biomolecules [26]. However, as noted above, TiO_2-g-C_3N_4 nano-composite exhibit admirable PEC performance with visible light excitation due to the unique electronic band structure between g-C_3N_4 (conduction band edges at −1.13 V, versus NHE) and TiO_2 (conduction band edges at −0.5 V, versus NHE), which improves the PEC performance of g-C_3N_4 [27]. These findings encourage the wider use of TiO_2-g-C_3N_4 composites in PEC biosensor development.

Metal-organic frameworks (MOFs) are porous coordination polymers, which have been researched intensively over the last decade due to their high specific surface areas and discrete pore sizes [28]. Among various MOFs, the zeolitic imidazole framework-8 (ZIF-8) with 2-methlylimidazole as the linker has been particularly researched due its facile synthesis, various cation formulations and excellent thermochemical stability which allow end applications in gas sorption, gas separation, catalysis and fluorescence analysis [29,30]. Recently, ZIF-8 was used in a PEC biosensor to increase the surface area of the active electrode [31], highlighting the potential for MOF integration into biosensor fabrication for enhanced sensitivity.

In our previous work on PKA activity assay using PEC technique, g-C_3N_4, its derivative and nanocomposite were employed as photoactive material [16,32]. For example, we once developed a PEC strategy for PKA activity assay based on the bond between phosphorylated peptide and phosphorylated graphite-like carbon nitride (P-g-C_3N_4) conjugates triggered by Zr^{4+} ion coordination [16]. Though this method is simple, the detection limit needs to be improved and the preparation of P-g-C_3N_4 is time-consumption. Another work had also been performed by us for PKA assay. In that work, the PEC biosensor was designed based on the blocked digestion ability of carboxypeptidase Y (CPY) on the substrate peptide after PKA-catalyzed phosphorylation reaction, signal amplification strategy triggered by PAMAM dendrimer and alkaline phosphatase (ALP, which catalyzes the hydrolysis reaction of its substrate to produce electron donor for the PEC biosensor), and photoactive material of TiO_2/g-C_3N_4 nanocomposite (which was modified on ITO electrode surface) [32]. However, the separation process for the phosphorylated substrate peptide is tedious, which makes the detection process is more complicated.

To solve these disadvantages, in this work, a simple PEC biosensor was constructed for protein kinase A (PKA) detection based on the specific catalytic effect of PKA towards its substrate peptide. To improve the sensitivity of the biosensor, carbon microspheres (CMS) and gold nanoparticle decorated ZIF-8 (Au-ZIF-8) were employed, with the Au-ZIF-8 also being used for the immobilization of the substrate peptide. To the best of our knowledge, Au-ZIF-8 nanocomposite was firstly employed in the fabrication of PEC biosensor for PKA activity assay. A TiO_2-g-C_3N_4 nanocomposite was employed as the photoactive material, with the TiO_2 serving as the recognition agent for phosphate groups resulting PKA catalytic action on the peptide (Which is different with our previous work. Here, TiO_2-g-C_3N_4 nanocomposite was captured on electrode surface by phosphorylated peptide). PKA detection therefore relied on the linear relationship between PKA concentration and photocurrent of the biosensor. The inhibition of PKA by ellagic acid was also investigated as a demonstration of the practicality of the PEC biosensor. Compared with our previous work on PKA detection based on PEC methods [16,32], the developed method shows merits of simple operation, easy fabrication of electrode, low cost and high detection sensitivity.

2. Experimental

2.1. Reagents and instruments

PKA, casein kinase I (CK1), casein kinase II (CK2), and p42 MAP Kinase (MAPK) were acquired from NEB (USA). Tris (hydroxymethyl) aminomethane (Tris), $HAuCl_4$, $Zn(NO_3)_2$, ascorbic acid (AA), 2-methyimidazole and tetrabutyltitanate were obtained from Aladdin (Shanghai, China). The short peptide with sequence of CRRLRRASLG and ATP were acquired from Sangon (China). Indium tin oxide (ITO) coated glass slides (coating thickness 180 ± 25 nm, sheet resistance < 15 U/cm^2) were purchased from Zhuhai Kaivo Electronic Components Co., Ltd. (Zhuhai, China).

The buffer solutions and instruments are described in Supplementary material.

2.2. Preparation of Au-ZIF-8

ZIF-8 was prepared according to a literature method with some mirror modifications [33]. Briefly, 0.585 g $Zn(NO_3)_2$ was dissolved in 4 mL sterile water. 11.35 g 2-methylimidazole was dissolved in 40 mL sterile water. Subsequently, the two solutions were then combined together under magnetic stirring for 5 min afterwards, the solution was centrifuged and the sediment was washed three times with deionized water. In the end, ZIF-8 product was dried under vacuum at 60 °C overnight.

To prepare Au-ZIF-8, 0.2 g ZIF-8 was added into 20 mL of a 10 mM $HAuCl_4$ solution, and the resulting dispersion stirred magnetically for 12 h at room temperature. Then, 0.2 M $NaBH_4$ solution (10 mL) was added into the $AuCl_4^-$/ZIF-8 dispersion under vigorous stirring, and the stirring continued for 30 min. Au-ZIF-8 product was washed with water and dried under vacuum at 60 °C.

2.3. Preparation of the TiO_2-g-C_3N_4 composite

g-C_3N_4 was prepared according to a literature report [34]. Briefly, 3.0 g dicyandiamide was put inside a porcelain boat, which was subsequently placed in a tube furnace. The furnace was first heated to 220 °C with a heating rate of 3 °C/min, then keep the temperature constant for 2 h. Next, the furnace was heated to 350 °C and keep at this temperature for 2 h. Finally, the furnace was heated to 550 °C and kept at this temperature for 4 h. The product was then cooled naturally to room temperature. The impure g-C_3N_4 product was collected and dispersed in deionized water under ultrasonication. After centrifuging at 12,000 rpm, the sediment was collected, which was further washed with ethanol to remove any organic impurities. This process of dispersion in water, centrifugation, washing with ethanol, centrifugation was repeated twice. Finally, the yellow g-C_3N_4 product was dried at 60 °C for 6 h.

The TiO_2-g-C_3N_4 nanocomposite was prepared using a hydrothermal synthesis technique [35]. Firstly, 966 mg g-C_3N_4 was dispersed in 2 mL tetrabutyl titanate, to which 60 mL of acetone was then added. After that, the resulting dispersion was introduced into a teflon-lined stainless steel autoclave and heated at 180 °C for 12 h. After cooling naturally to room temperature, the solid product was collected by centrifugation and washed successively with deionized water and then acetone three times. Finally, the TiO_2-g-C_3N_4 nanocomposite was dried at 60 °C for 6 h.

2.4. Preparation of CMS

CMS were synthesized using a literature method [36]. Glucose (3.2 g) was firstly dissolved in 70 mL deionized water. Then, the

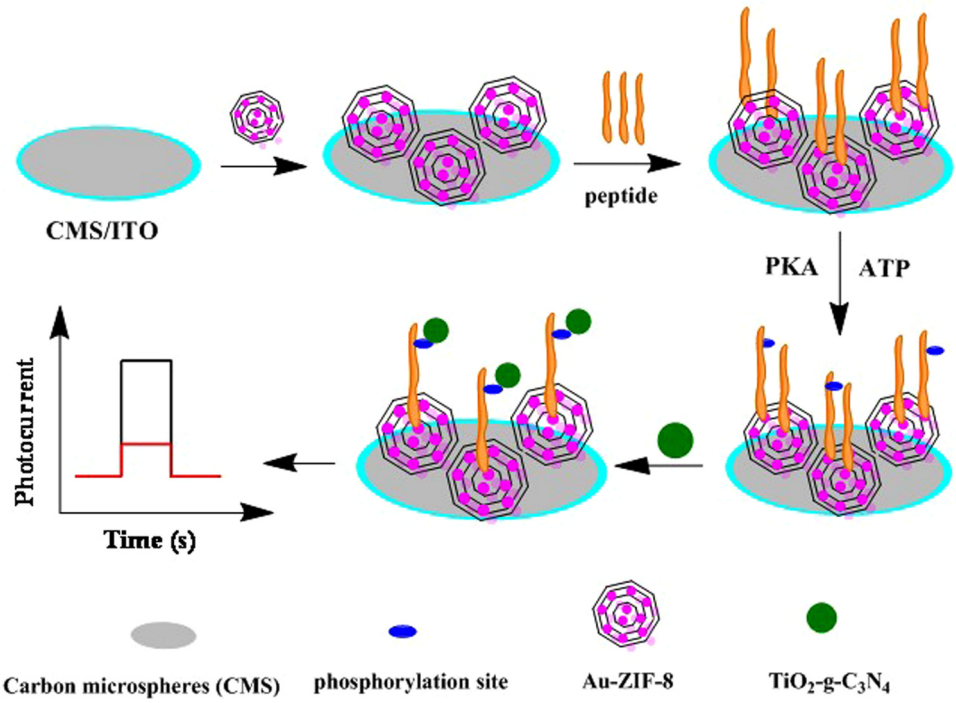

Scheme 1. Schematic representation of the construction of the PEC biosensor.

solution was added into a Teflon-lined stainless steel autoclave and heated at 180 °C for 3 h. After cooling to room temperature, the black sediment was obtained with centrifugation. Subsequently, the sediment was washed with ethanol and deionized water for three times, respectively. Finally, CMS product was dried under vacuum at 60 °C for 6 h.

2.5. Fabrication of the PEC biosensor

To fabricate the PEC biosensor, the ITO electrode was successively cleaned by ultrasonication for 15 min in acetone and 1 M NaOH solution (in 50 vol% ethanol) and finally in distilled water. The electrode was dried at room temperature. A CMS dispersion was prepared by ultrasonically dispersing 2 mg CMS in 1 mL deionized water. 40 μL of CMS dispersion was carefully dropped onto ITO electrode surface. After dried, the prepared electrode was denoted as CMS/ITO. The electrode was then rinsed with deionized water and dried with N_2 flow. Subsequently, 40 μL of a 3 mg mL^{-1} Au-ZIF-8 dispersion (in water) was dropped onto the CMS/ITO electrode surface and dried under the infrared lamp, followed by rinsing with deionized water and drying under N_2 (the obtained electrode was named Au-ZIF-8/CMS/ITO). Afterwards, the Au-ZIF-8/CMS/ITO was incubated in 40 μL of peptide immobilization buffer containing 1 μM peptide. After 12 h, the electrode was rinsed with washing buffer for three times to remove any non-immobilized peptide (the resulting electrode is denoted as peptide/Au-ZIF-8/CMS/ITO). The immobilized peptide was then phosphorylated via PKA catalysis. Briefly, peptide/Au-ZIF-8/CMS/ITO was incubated with 40 μL of PKA reaction buffer containing various concentrations of PKA at 37 °C for 40 min. Subsequently, the electrode was rinsed thoroughly with washing buffer. The obtained electrode is denoted as P-peptide/Au-ZIF-8/CMS/ITO. Next, 40 μL of a 2 mg mL^{-1} TiO_2-g-C_3N_4 dispersion was casted onto the surface of P-peptide/Au-ZIF-8/CMS/ITO and incubated for 1 h. The obtained electrode (TiO_2-g-C_3N_4/P-peptide/Au-ZIF-8/CMS/ITO) was rinsed with washing buffer three times.

2.6. Inhibition assay

3 × PKA reaction buffers containing series concentrations of ellagic acid were prepared. Then, the PEC biosensor was fabricated according to the process described in Section 2.5 except that the PKA reaction buffer was replaced by the buffers containing ellagic acid. The inhibition ratio was evaluated according to the equation of Inhibition ratio (%) = $(I_3\text{-}I_2)/(I_3\text{-}I_1)$. In this equation, I_3 was the photocurrent of TiO_2-g-C_3N_4/P-Peptide/Au-ZIF-8/CMS/ITO without inhibitor, I_2 was the photocurrent of TiO_2-g-C_3N_4/P-Peptide/Au-ZIF-8/CMS/ITO with inhibitor, and I_1 was the photocurrent of Peptide/Au-ZIF-8/CMS/ITO.

3. Results and discussion

3.1. Detection strategy

The fabrication of the PEC biosensor and detection strategy for PKA are described in Scheme 1. Firstly, CMS were immobilized on the pretreated ITO electrode surface. CMS were used here to increase the electrode area and also improve the conductivity of the bare ITO electrode. Au-ZIF-8 was then deposited on the CMS/ITO electrode, with the Au-ZIF-8 subsequently used for immobilization of the substrate peptide (via bonding between Au and –SH groups on cysteine residues of the peptide). In the presence of ATP, PKA catalyzed the phosphorylation of serine residues on the substrate peptide. Finally, relying on specific interactions between TiO_2 and phosphate groups, the TiO_2-g-C_3N_4 nanocomposite was modified on P-Peptide/Au-ZIF-8/CMS/ITO surface. With visible light, g-C_3N_4 was photoexcited, giving the assembled biosensor a strong PEC response. The photocurrent generated is dependent on the phosphorylated degree of peptide, which in turn is influenced by the concentration of PKA. Based on the connection between PKA concentration and photocurrent, PKA can be detected and quantified.

3.2. Characterization of CMS, TiO_2-g-C_3N_4 and Au-ZIF-8

The morphologies of CMS, TiO_2-g-C_3N_4 and Au-ZIF-8 were characterized by TEM. As shown in Fig. 1A, CMS possessed a spherical structure. Au-ZIF-8 comprised small gold nanoparticles (mean diameter ~5 nm) uniformly dispersed over the surface of ZIF-8 crystals of size 50–80 nm (Fig. 1B). The TiO_2-g-C_3N_4 composite consisted of g-C_3N_4 sheets richly decorated with 10–15 nm anatase TiO_2 nanoparticles (Fig. 1C).

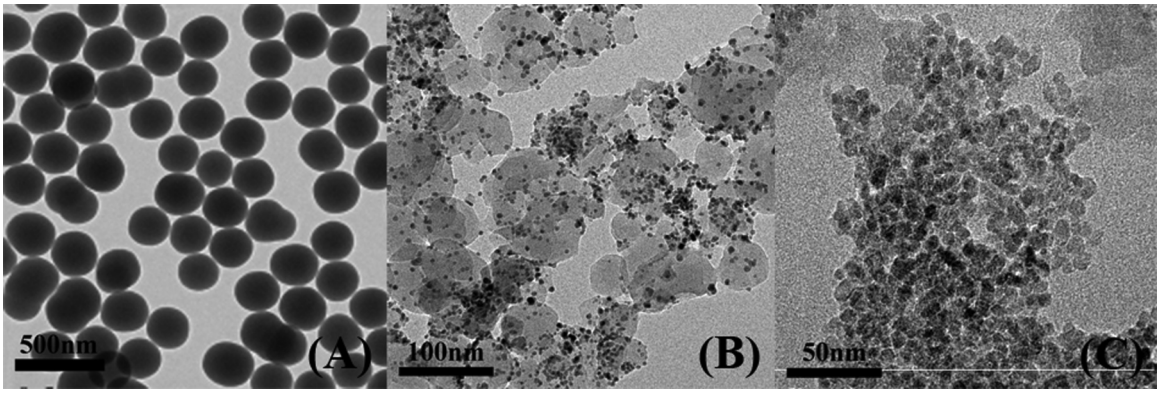

Fig. 1. TEM images of CMS (A), Au-ZIF-8 (B) and TiO_2-g-C_3N_4(C).

3.3. EIS characterization and detection feasibility assay

To monitor the stepwise modification process, EIS was performed on the electrodes after each fabrication step. The corresponding EIS curves are shown in Fig. 2A. Curve a is for the ITO electrode, which afforded an electron transfer resistance (R_{et}) of 60 Ω. As for CMS/ITO, the R_{et} value decreased (curve b), which can be rationalized in terms of the increased electrode surface area and improved electrode conductivity. The R_{et} value increased when Au-ZIF-8 was deposited on the CMS/ITO surface (curve c), which is explained to the increased diffusion route of $Fe(CN)_6^{3-/4-}$ to CMS/ITO surface and also increased interface electron transfer resistance. R_{et} increased again when the peptides were modified on Au-ZIF-8/CMS/ITO surface, which was expected due to the enhanced steric-hindrance effect caused by the immobilized peptide (curve d). The R_{et} value further enhanced when peptides were phosphorylated by PKA (curve e). In which, a phosphate group is transferred to the serine residue of the substrate peptide, thereby increasing the negative charge of the peptide and repelling $Fe(CN)_6^{3-/4-}$ diffusion. After binding of TiO_2-g-C_3N_4 through TiO_2-phosphate group interactions, the R_{et} value increased greatly (curve f), indicating the further hindrance of the diffusion of $Fe(CN)_6^{3-/4-}$ by the bulky TiO_2-g-C_3N_4. According to the changes of the R_{et} values with each stage of biosensor fabrication, the successful fabrication of the TiO_2-g-C_3N_4/P-Peptide/Au-ZIF-8/CMS/ITO biosensor was verified.

The detection feasibility was investigated by comparing the PEC response of the different modified electrodes in the PEC detection buffer. The results were shown in Fig. 2B. No PEC response was achieved at the bare ITO electrode (curve a), implying that ITO had negligible photoactivity under visible light. CMS/ITO showed a very weak photocurrent (curve b), indicating that CMS possessed weak photoactivity which was not surprising given their dark color. After electrode modification with Au-ZIF-8, the photocurrent improved slightly (curve c). It can be attributed to stimulation of the localized surface plasmon resonance of AuNPs under visible light, resulting in subsequent electron transfer from the AuNPs to the CMS/ITO electrode. However, when the substrate peptide was assembled on Au-ZIF-8/CMS/ITO surface (curve d), and then phosphorylated via PKA (curve e), the photocurrent successively decreased. This decrease can be ascribed to the increased steric-hindrance effect originated from the substrate peptide and the increased negative charge resulted from the introduced phosphate groups. The photocurrent increased greatly when TiO_2-g-C_3N_4 was captured on P-peptide/Au-ZIF-8/CMS/ITO surface (curve f). This increase is explained by introducing g-C_3N_4 which is a good photoactive material under visible light (especially when composited with TiO_2 due to the enhanced charge separation that results). To confirm the crucial role of PKA in the fabrication of the biosensor, the electrode peptide/Au-ZIF-8/CMS/ITO was incubated directly with TiO_2-g-C_3N_4 (curve g). The obtained photocurrent was much lower than that determined for the TiO_2-g-C_3N_4/peptide/Au-ZIF-8/CMS/ITO. It can therefore be concluded that without PKA phosphorylation of the peptide, TiO_2-g-C_3N_4 cannot be immobilized effectively due to the absence of phosphate groups on the peptide (phosphate binds very strongly on TiO_2 surfaces). The data in Fig. 2B confirms the detection feasibility of the developed method for PKA.

3.4. PKA detection

Under the optimized testing conditions (see Supplementary material), the photocurrent response was measured at various PKA

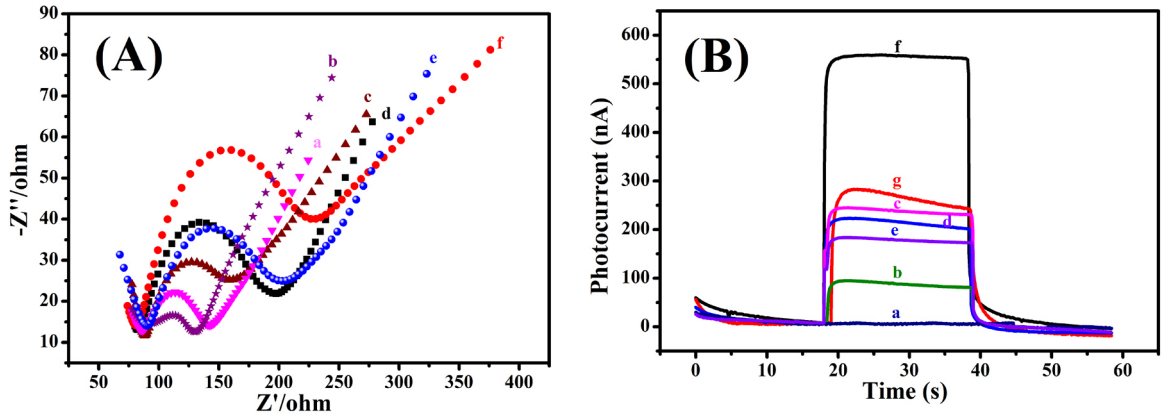

Fig. 2. (A) The Nyquist plot for different electrodes in 10 mM Tris-HCl (pH 7.5) containing 5 mM $K_3[Fe(CN)_6]/K_4[Fe(CN)_6]$ (1:1 M ratio) and 0.1 M KCl over the frequency range of 10^{-1}–10^5 Hz: (a) ITO, (b) CMS/ITO, (c) Au-ZIF-8/CMS/ITO, (d) Peptide/Au-ZIF-8/CMS/ITO, (e) P-Peptide/Au-ZIF-8/CMS/ITO, and (f) TiO_2-g-C_3N_4/P-Peptide/Au-ZIF-8/CMS/ITO. (B) PEC response of different electrodes in the detection buffer. (a) ITO, (b) CMS/ITO, (c) Au-ZIF-8/CMS/ITO, (d) Peptide/Au-ZIF-8/CMS/ITO, (e) P-Peptide/Au-ZIF-8/CMS/ITO, (f) TiO_2-g-C_3N_4/P-Peptide/Au-ZIF-8/CMS/ITO, and (g) Peptide/Au-ZIF-8/CMS/ITO incubated with TiO_2-g-C_3N_4.

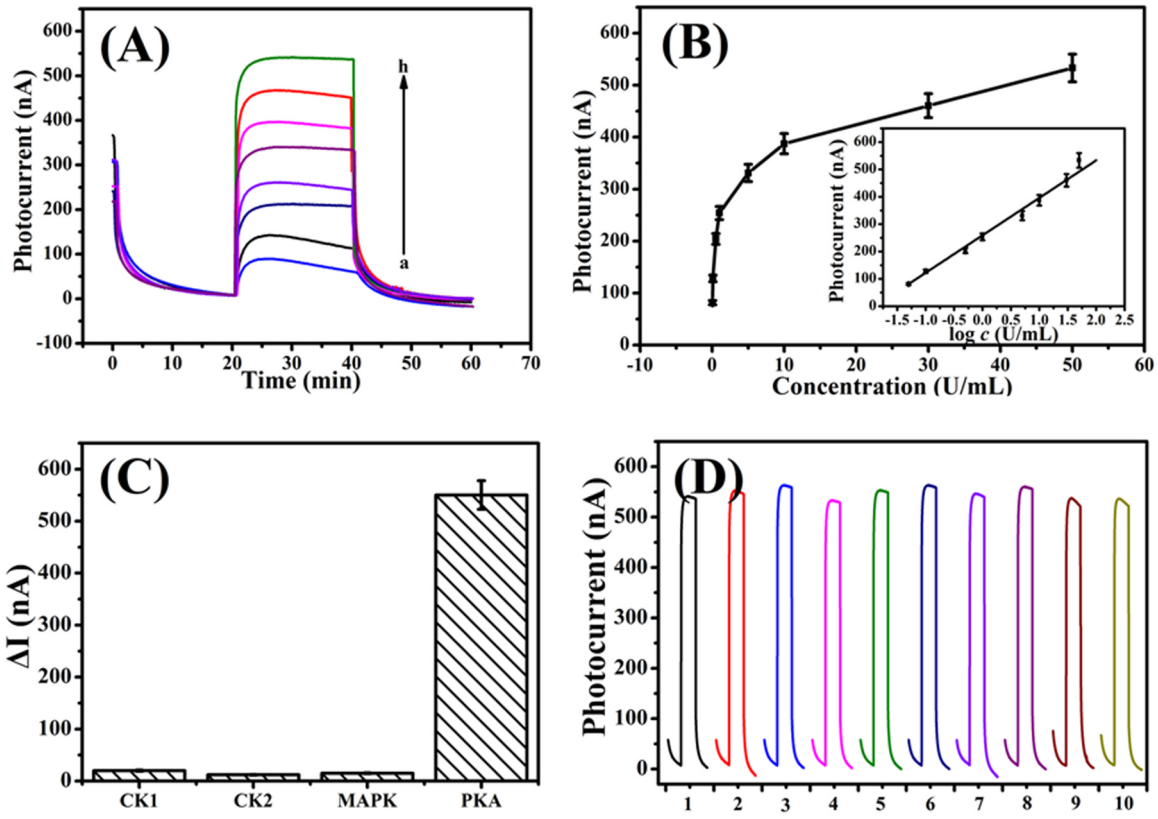

Fig. 3. (A) The PEC response of the biosensor with different PKA concentrations. a – j, 0.05, 0.1, 0.5, 1, 5, 10, 30, 50 U mL^{-1}. (B) Plot for the relationship between the photocurrent and PKA concentration from 0.05 to 50 U mL^{-1}. Insert, the linear relationship between the photocurrent and the logarithm of PKA concentration from 0.05 to 50 U mL^{-1}. (C) The photocurrent change after the biosensor was fabricated with different kinases (50 U mL^{-1}). (D) The photocurrent for ten biosensors fabricated independently. The PKA concentration was 50 U mL^{-1}.

concentrations. On increasing PKA concentration from 0.05 to 50 U mL^{-1}, the photocurrent increased reaching a saturation value around 50 U mL^{-1} (Fig. 3A). A good linear relationship was established between the photocurrent and PKA concentration from 0.05 to 50 U mL^{-1} (Fig. 3B), as described by the linear regression equation I (nA) = 133.95$logc$ + 256.204 (R^2 = 0.992). The detection limit was 0.02 U mL^{-1} (S/N = 3). With regard to detection sensitivity, the developed PKA detection method was superior to most previously reported PKA sensors (see Table 1), indicating that the developed methods might be a viable detection platform for PKA.

The selectivity and reproducibility of a biosensor are essential criteria for potential application. To assess the specificity of the PEC method, three protein kinases were used as potential interferants, with all other biosensor fabrication processes the same as described in Section 2.5. The photocurrent change ($\Delta I = I_1$-I_2) was compared, where I_1 is the photocurrent of the biosensor fabricated with different protein kinases (concentration 50 U mL^{-1}) and I_2 is the photocurrent of peptide/Au-ZIF-8/CMS/ITO. As can be from Fig. 3C, the ΔI for PKA was much higher than those obtained using the other protein kinases, indicating that this PEC biosensor has excellent detection specificity for PKA. To investigate reproducibility of this method, ten PEC biosensors were fabricated independently via the same stepwise process. The relative standard deviation (RSD) in the photocurrent was only 2.03% (Fig. 3D), implying very good detection reproducibility. In addition, the reproducibility for the slope of the calibration curve was also investigated. For five calibration curves, the RSD for these five slopes is 6.58%, indicating acceptable reproducibility.

The stability of the developed method should also be clarified. To investigate it, the fabricated biosensor was applied to detect 10 U mL^{-1} PKA by weekly recording its photoelectrochemical response for two weeks. The biosensor can remain 96.37% and 91.58% of its original response after on e and two weeks, respectively. This results indicate the acceptable stability.

Table 1
Comparison of PKA detection performance of various methods.

Methods	Kinase	Linear range (U mL^{-1})	LOD (U mL^{-1})	Refs.
Photoluminescent	CK2	0.1–1	0.03	[37]
Electrochemistry	EGFR	2–100	1	[38]
Electrochemistry	PKA	0.05–100	0.014	[12]
Electrochemistry	PKA	0.005–50	0.002	[11]
Electrochemistry	CK2	0.1–10	0.047	[39]
Electrochemistry	PKA	0.1–1	0.09	[40]
Colorimetry	PKA	0.1–0.5	0.0375	[8]
Fluorescence	PKA	0–400	0.47	[41]
Fluorescence	PKA	0–1000	0.5	[42]
Fluorescence	PKA	0–800	0.5	[43]
Fluorescence	PKA	1–2000	0.5	[44]
QCM	PKA	0.64–22.33	0.061	[45]
ECL	PKA	5–500	0.5	[46]
ECL	PKA	0.07–32	0.07	[47]
PEC method	PKA	0.005–0.0625	0.0049	[15]
PEC method	PKA	0.05–100	0.048	[32]
PEC method	PKA	0.05–50	0.077	[16]
PEC method	PKA	0.05–100	0.017	[48]
PEC method	PKA	0.05–100	0.015	[49]
PEC method	PKA	0.05–50	0.02	This work

3.5. Inhibition assay

To verify the applicability of this test method, the effect of ellagic acid concentration on PKA activity was investigated. Fig. 4A shows that the photocurrent decreased with increasing ellagic acid concentration, indicating that ellagic acid can effectively inhibit the catalytic activity

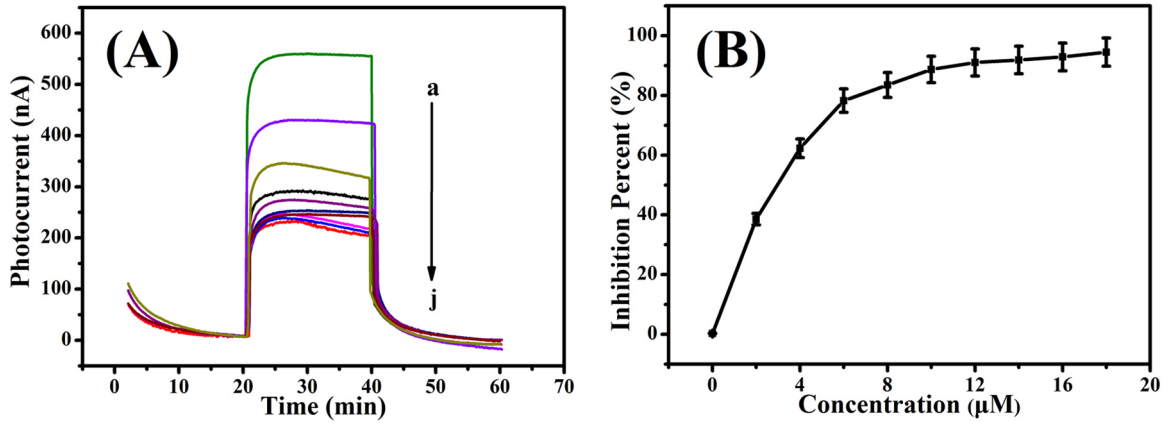

Fig. 4. (A) PEC response of the biosensor with different concentrations of ellagic acid. a − j 0, 2, 4, 6, 8, 10, 12, 14, 16, and 18 μM. The PKA concentration was 50 U mL^{-1}. (B) Plot showing the relationship between the ellagic acid concentration and the inhibition percentage.

Table 2
Assay of PKA activity on HepG-2 cell lysate.

Sample	Added (U mL^{-1})	Founded (U mL^{-1})	Recovery (%)	RSD (%)
1	0	–	–	–
2	5	5.28	105.6	8.47
3	10	9.35	93.5	6.14
4	20	21.58	107.9	3.25

of PKA. The inhibition percentage increased with ellagic acid concentration in the range 0–12 μM, and then leveled off at higher concentrations due to saturation inhibition (Fig. 4B). The IC_{50} value (the half-maximum inhibitory concentration) was 5.2 μM, which was comparable with values found in previous work [16,46,50]. The data indicates that this detection platform can be used to screen protein kinase inhibitors, thereby suggesting great potential for kinase-targeted drug discovery.

3.6. PKA detection in cell lysate

To further investigate the applicability of the developed method for PKA detection in real sample, PKA activity in HepG-2 cell lysate was analyzed with standard addition method. As listed in Table 2, no PKA activity was detected in blank cell lysate, which might be caused by that there is no PKA in cell lysate or PKA activity in cell lysate is low then the detection limit of our work. For detecting the added PKA, the results show that the recoveries is ranged from 93.5% to 107.9% and the RSD is ranged from 3.25% to 8.47%, which implies satisfactory applicability of the developed method for PKA detection in cell lysate.

4. Conclusion

In conclusion, a sensitive PEC biosnesor was constructured for PKA detection and inhibitor screening. The sensitivity originated from the successful integration of CMS which increased the electrode surface area, Au-ZIF-8 which provided the immobilization site for the substrate peptide, and the TiO_2-g-C_3N_4 nanocomposite which greatly enhanced the PEC response. The developed method offered a linear response over a wide PKA concentration range and a low detection limit. Because this method was based on the specific catalytic ability of PKA towards its unique substrate peptide, the PEC biosensor showed very high detection selectivity. Furthermore, the biosensor shows great potential in the kinase inhibitor screening. Finally, by changing the substrate peptide, it should be possible to extend this approach and develop PEC biosensors for the detection and inhibition screening of other kinases.

Acknowledgement

This work was supported by the National Natural Science Foundation of China (Nos. 21775090, 21375079), the Natural Science Foundation of Shandong Province, China (No. ZR2014BQ029). GINW acknowledges funding support from the Ministry of Business Innovation and Employment (MBIE) Catalyst Fund, Contract MAUX1609: "Disruptive Technologies from Metal-Organic Frameworks".

Notes

The authors declare no competing financial interest.

Appendix A. Supporting information

Supplementary data associated with this article can be found in the online version at doi:10.1016/j.talanta.2018.12.035.

References

[1] A. Dupre, E.M. Daldello, A.C. Nairn, C. Jessus, O. Haccard, Phosphorylation of ARPP19 by protein kinase A prevents meiosis resumption in Xenopus oocytes, Nat. Commun. 5 (2014) 3318.
[2] Z. Yan, Z. Wang, Z. Miao, Y. Liu, Dye-sensitized and localized surface plasmon resonance enhanced visible-light photoelectrochemical biosensors for highly sensitive analysis of protein kinase activity, Anal. Chem. 88 (2016) 922–929.
[3] P.J. Roberts, C.J. Der, Targeting the Raf-MEK-ERK mitogen-activated protein kinase cascade for the treatment of cancer, Oncogene 26 (2007) 3291–3310.
[4] S.A. Beausoleil, J. Villén, S.A. Gerber, J. Rush, S.P. Gygi, A probability-based approach for high-throughput protein phosphorylation analysis and site localization, Nat. Biotechnol. 24 (2006) 1285–1292.
[5] M. Wang, L. Wang, Q. Liu, X. Su, A fluorescence sensor for protein kinase activity detection based on gold nanoparticles/copper nanoclusters system, Sens. Actuators B-Chem. 256 (2018) 691–698.
[6] T. Hayama, E. Kiyokawa, H. Yoshida, O. Imakyure, M. Yamaguchi, H. Nohta, Fluorous-assisted metal chelate affinity extraction technique for analysis of protein kinase activity, Talanta 156–157 (2016) 1–5.
[7] H. Kitazaki, T. Mori, J.-H. Kang, T. Niidome, M. Murata, M. Hashizume, Y. Katayama, A colorimetric assay of protein kinase activity based on peptide-induced coagulation of gold nanorods, Colloid Surf. B 99 (2012) 7–11.
[8] C. Shen, K. Zhang, N. Gao, S. Wei, G. Liu, Y. Chai, M. Yang, Colorimetric and electrochemical determination of the activity of protein kinase based on retarded particle growth due to binding of phosphorylated peptides to DNA-ccapped silver nanoclusters, Microchim Acta 183 (2016) 2933–2939.
[9] T. Li, D. Liu, Z. Wang, Microarray-based Raman spectroscopic assay for kinase inhibition by gold nanoparticle probes, Biosens. Bioelectron. 24 (2009) 3335–3339.
[10] K. Inamori, M. Kyo, Y. Nishiya, Y. Inoue, T. Sonoda, E. Kinoshita, T. Koike, Y. Katayama, Detection and quantification of on-chip phosphorylated peptides by surface plasmon resonance imaging techniques using a phosphate capture molecule, Anal. Chem. 77 (2005) 3979–3985.
[11] C. Shen, X. Li, A. Rasooly, L. Guo, K. Zhang, M. Yang, A single electrochemical biosensor for detecting the activity and inhibition of both protein kinase and alkaline phosphatase based on phosphate ions induced deposition of redox precipitates, Biosens. Bioelectron. 85 (2016) 220–225.
[12] Y. Zhou, H. Yin, X. Li, Z. Li, S. Ai, H. Lin, Electrochemical biosensor for protein

kinase A activity assay based on gold nanoparticles-carbon nanospheres, phos-tag-biotin and β-galactosidase, Biosens. Bioelectron. 86 (2016) 508–515.
[13] Y. Zhou, M. Wang, H. Yin, S. Ai, Amperometric determination of the activity of protein kinase a using a glassy carbon electrode modified with IgG functionalized gold nanoparticles conjugated to horseradish peroxidase, Microchim Acta 184 (2017) 3301–3308.
[14] R.-P. Liang, W.-B. Qiu, H.-F. Zhao, C.-Y. Xiang, J.-D. Qiu, Electrochemiluminescence resonance energy transfer between graphene quantum dots and graphene oxide for sensitive protein kinase activity and inhibitor sensing, Anal. Chim. Acta 904 (2016) 58–64.
[15] Z. Wang, Z. Yan, F. Wang, J. Cai, L. Guo, J. Su, Y. Liu, Highly sensitive photoelectrochemical biosensor for kinase activity detection and inhibition based on the surface defect recognition and multiple signal amplification of metal-organic frameworks, Biosens. Bioelectron. 97 (2017) 107–114.
[16] X. Li, Y. Zhou, Y. Xu, H. Xu, M. Wang, H. Yin, S. Ai, A novel photoelectrochemical biosensor for protein kinase activity assay based on phosphorylated graphite-like carbon nitride, Anal. Chim. Acta 934 (2016) 36–43.
[17] X. Wang, P. Gao, T. Yan, R. Li, R. Xu, Y. Zhang, B. Du, Q. Wei, Ultrasensitive photoelectrochemical immunosensor for insulin detection based on dual inhibition effect of CuS-SiO_2 composite on CdS sensitized C-TiO_2, Sens. Actuators B-Chem. 258 (2018) 1–9.
[18] W.-W. Zhao, J.-J. Xu, H.-Y. Chen, Photoelectrochemical enzymatic biosensors, Biosens. Bioelectron. 92 (2017) 294–304.
[19] Y. Li, L. Sun, Q. Liu, E. Han, N. Hao, L. Zhang, S. Wang, J. Cai, K. Wang, Photoelectrochemical CaMV35S biosensor for discriminating transgenic from non-transgenic soybean based on SiO_2@CdTe quantum dots core-shell nanoparticles as signal indicators, Talanta 161 (2016) 211–218.
[20] H. Ye, H. Wang, B. Zhang, F. Zhao, B. Zeng, Tremella-like $ZnIn_2S_4$/graphene composite based photoelectrochemical sensor for sensitive detection of dopamine, Talanta 186 (2018) 459–466.
[21] Y. Wang, Y. Zhou, L. Xu, Z. Han, H. Yin, S. Ai, Photoelectrochemical apta-biosensor for zeatin detection based on graphene quantum dots improved photoactivity of graphite-like carbon nitride and streptavidin induced signal inhibition, Sens. Actuators B-Chem. 257 (2018) 237–244.
[22] R. Motaghed Mazhabi, L. Ge, H. Jiang, X. Wang, A facile photoelectrochemical sensor for high sensitive ROS and AA detection based on graphitic carbon nitride nanosheets, Biosens. Bioelectron. 107 (2018) 54–61.
[23] M. Amouzadeh Tabrizi, M. Shamsipur, R. Saber, S. Sarkar, V. Ebrahimi, A high sensitive visible light-driven photoelectrochemical aptasensor for shrimp allergen tropomyosin detection using graphitic carbon nitride-TiO_2 nanocomposite, Biosens. Bioelectron. 98 (2017) 113–118.
[24] X. Ma, Y. Wei, Z. Wei, H. He, C. Huang, Y. Zhu, Probing π-π stacking modulation of g-C_3N_4/graphene heterojunctions and corresponding role of graphene on photocatalytic activity, J. Colloid Interface. Sci. 508 (2017) 274–281.
[25] X. Chen, H. Li, Y. Wu, H. Wu, L. Wu, P. Tan, J. Pan, X. Xiong, Facile fabrication of novel porous graphitic carbon nitride/copper sulfide nanocomposites with enhanced visible light driven photocatalytic performance, J. Colloid Interface Sci. 476 (2016) 132–143.
[26] Z. Fan, L. Fan, S. Shuang, C. Dong, Highly sensitive photoelectrochemical sensing of bisphenol A based on zinc phthalocyanine/TiO_2 nanorod arrays, Talanta 189 (2018) 16–23.
[27] F.X. Wang, C. Ye, S. Mo, L.L. Liao, X.F. Zhang, Y. Ling, L. Lu, H.Q. Luo, N.B. Li, A novel "signal-on" photoelectrochemical sensor for ultrasensitive detection of alkaline phosphatase activity based on a TiO_2/g-C_3N_4 heterojunction, Analyst 143 (2018) 3399–3407.
[28] C. Hou, G. Zhao, Y. Ji, Z. Niu, D. Wang, Y. Li, Hydroformylation of alkenes over rhodium supported on the metal-organic framework ZIF-8, Nano Res. 7 (2014) 1364–1369.
[29] H. Yin, H. Kim, J. Choi, A.C.K. Yip, Thermal stability of ZIF-8 under oxidative and inert environments: a practical perspective on using ZIF-8 as a catalyst support, Chem. Eng. J. 278 (2015) 293–300.
[30] K. Wang, H. Ren, N. Li, X. Tan, F. Dang, Ratiometric fluorescence sensor based on cholesterol oxidase-functionalized mesoporous silica nanoparticle@ZIF-8 core-shell nanocomposites for detection of cholesterol, Talanta 188 (2018) 708–713.
[31] R. Yang, X. Yan, Y. Li, X. Zhang, J. Chen, Nitrogen-doped porous carbon-ZnO nanopolyhedra derived from ZIF-8: new materials for photoelectrochemical biosensors, ACS Appl. Mater. Interfaces 9 (2017) 42482–42491.
[32] X. Li, L. Zhu, Y. Zhou, H. Yin, S. Ai, Enhanced photoelectrochemical method for sensitive detection of protein kinase A activity using TiO_2/g-C_3N_4, PAMAM dendrimer, and alkaline phosphatase, Anal. Chem. 89 (2017) 2369–2376.
[33] L. Shi, X. Zhu, T. Liu, H. Zhao, M. Lan, Encapsulating Cu nanoparticles into metal-organic frameworks for nonenzymatic glucose sensing, Sens. Actuators B-Chem. 227 (2016) 583–590.
[34] H. Li, Y. Liu, Y. Cui, W. Zhang, C. Fu, X. Wang, Facile synthesis and enhanced visible-light photoactivity of $DyVO_4$ /g-C_3N_4 I composite semiconductors, Appl. Catal. B: Environ. 183 (2016) 426–432.
[35] J. Tian, R. Ning, Q. Liu, A.M. Asiri, A.O. Al-Youbi, X. Sun, Three-dimensional porous supramolecular architecture from ultrathin g-C_3N_4 nanosheets and reduced graphene oxide: solution self-assembly construction and application as a highly efficient metal-free electrocatalyst for oxygen reduction reaction, ACS Appl. Mater. Interface 6 (2014) 1011–1117.
[36] Y. Mi, W. Hu, Y. Dan, Y. Liu, Synthesis of carbon micro-spheres by a glucose hydrothermal method, Mater. Lett. 62 (2008) 1194–1196.
[37] Y. Wang, L. Zhang, R.P. Liang, J.M. Bai, J.D. Qiu, Using graphene quantum dots as photoluminescent probes for protein kinase sensing, Anal. Chem. 85 (2013) 9148–9155.
[38] Y. Yang, L.H. Guo, N. Qu, M.Y. Wei, L.X. Zhao, B. Wan, Label-free electrochemical measurement of protein tyrosine kinase activity and inhibition based on electrocatalyzed tyrosine signaling, Biosens. Bioelectron. 28 (2011) 284–290.
[39] H. Yin, X. Wang, Y. Guo, Y. Zhou, S. Ai, Electrochemical detection of protein kinase activity based on carboxypeptidase Y digestion triggered signal amplification, Biosens. Bioelectron. 66 (2015) 77–83.
[40] J. Liu, X. He, K. Wang, Y. Wang, G. Yan, Y. Mao, Amplified electrochemical detection of protein kinase activity based on gold nanoparticles/multi-walled carbon nanotubes nanohybrids, Talanta 129 (2014) 328–335.
[41] X. Xu, X. Liu, Z. Nie, Y. Pan, M. Guo, S. Yao, Label-free fluorescent detection of protein kinase activity based on the aggregation behavior of unmodified quantum dots, Anal. Chem. 83 (2011) 52–59.
[42] G. Lu, P. Tan, C. Lei, Z. Nie, Y. Huang, S. Yao, Fluorescent detection of protein kinase based on positively charged gold nanoparticles, Talanta 128 (2014) 360–365.
[43] P. Tan, C. Lei, X. Liu, M. Qing, Z. Nie, M. Guo, Y. Huang, S. Yao, Fluorescent detection of protein kinase based on zirconium ions-immobilized magnetic nanoparticles, Anal. Chim. Acta 780 (2013) 89–94.
[44] C. Shen, X. Xia, S. Hu, M. Yang, J. Wang, Silver nanoclusters-based fluorescence assay of protein kinase activity and inhibition, Anal. Chem. 87 (2015) 693–698.
[45] X. Xu, J. Zhou, X. Liu, Z. Nie, M. Qing, M. Guo, S. Yao, Aptameric peptide for one-step detection of protein kinase, Anal. Chem. 84 (2012) 4746–4753.
[46] P. Miao, L. Ning, X. Li, P. Li, G. Li, Electrochemical strategy for sensing protein phosphorylation, Bioconjugate Chem. 23 (2011) 141–145.
[47] S. Xu, Y. Liu, T. Wang, J. Li, Highly sensitive electrogenerated chemiluminescence biosensor in profiling protein kinase activity and inhibition using gold nanoparticle as signal transduction probes, Anal. Chem. 82 (2010) 9566–9572.
[48] Y. Zhou, M. Wang, Z. Yang, H. Yin, S. Ai, A Phos-tag-based photoelectrochemical biosensor for assay of protein kinase activity and inhibitors, Sens. Actuators, B 206 (2015) 728–734.
[49] H. Yin, B. Sun, L. Dong, B. Li, Y. Zhou, S. Ai, A signal "on" photoelectrochemical biosensor for assay of protein kinase activity and its inhibitor based on graphite-like carbon nitride, Phos-tag and alkaline phosphatase, Biosens. Bioelectron. 64 (2015) 462–468.
[50] Z. Chen, X. He, Y. Wang, K. Wang, Y. Du, G. Yan, Ru(II) encapsulated phosphorylate-terminated silica nanoparticles-based electrochemiluminescent strategy for label-free assay of protein kinase activity and inhibition, Biosens. Bioelectron. 41 (2013) 519–525.